Original Manuscript

Journal of Vibration and Control
2025, Vol. 0(0) 1–11

DOI: 10.1177/10775463251387454
journals.sagepub.com/home/jvc
Sage

Damping characterisation for 3D-printed polymeric structure with different geometric parameters

Feiyang He[1], Wanying Fan[2] and Muhammad Khan[1]

Abstract

This paper presents an experimental investigation into the influence of infill patterns and geometric angles on the damping properties of polymeric structures fabricated using fused deposition modelling (FDM). It quantitatively modelled the impact of geometric attributes of infill patterns on structural damping behaviours for the first time. The application of FDM highlights the ability to artificially control material damping without changing structural dimensions. Therefore, it has the potential to be used to fabricate customised polymer structures for energy absorption and vibration suppression applications. In the presented research, impact tests were conducted to assess the fundamental damping ratios of 3D-printed Polylactic acid (PLA) cantilever beams featuring various infill patterns (grid, triangle, and hexagon) and geometric angles. Notably, the triangle infill pattern with a filament angle of 60° exhibited the highest damping ratio, reaching up to 0.0163. Furthermore, an empirical model was developed and validated to establish a relationship between infill angles and fundamental damping ratios. The grid and hexagon patterns demonstrated promising results during the model validation phase.

Keywords

damping ratio, 3D printing, infill pattern, material extrusion, filament angle

Received: 17 February 2025; accepted: 26 September 2025

Introduction

3D printing was developed in the late 1980s. Nowadays, it plays an important role in a wide range of industries after more than 40 years of development (Aimar et al., 2019; Baqasah et al., 2019a; He et al., 2021; Joshi and Sheikh, 2015). Compared to traditional manufacturing methods, 3D printing technology can not only rapidly fabricate the product with complex and fine structure but also realise efficient manufacturing with different materials to meet the requirements of the functions and performance (Baqasah et al., 2019b; Francese et al., 2023; He et al., 2022). Meanwhile, since the rapid progress of technologies such as automotive (Narang et al., 2024), aerospace (Kaushik et al., 2023), high-speed delivery vehicles, and atomic energy has put forward higher requirements for the damping resistance of materials, as a new manufacturing technology, 3D printing has provided new ideas for improving the damping resistance of parts (Li et al., 2023). Therefore, academia and industry are interested in improving 3D-printed products' structural performance (Asli et al., 2024; Azouz et al., 2023).

Comprehensive studies investigated the effect of different materials and processing parameters on static mechanical properties such as stiffness and strength of printed products (Abusabir et al., 2022; Almutairi et al., 2023; Deswal et al., 2024; Hassanieh et al., 2021; He and Khan, 2021; Torrado et al., 2015; Vanaei et al., 2022). Some papers focused on surface dimensional accuracy (Atwah et al., 2022; Atwah and Khan, 2023; Chan et al., 2023; He et al., 2023; Kaushik and Garg, 2023; Shams et al., 2021a, 2021b). However, there is relatively less research on the damping properties of 3D-printed products. Damping is a physical phenomenon of energy dissipation over time due to the obstruction of an oscillating or vibrating system (Fundamental et al., 2024). As a new functional material, high-damping materials have wide applications in fields

[1]Centre for Life-cycle Engineering and Management, Cranfield University, Cranfield, United Kingdom of Great Britain and Northern Ireland
[2]School of Aerospace, Transport and Manufacturing, Cranfield University, Cranfield, United Kingdom of Great Britain and Northern Ireland

Corresponding author:
Muhammad Khan, B50, Centre for Life-cycle Engineering and Management, Cranfield University, Cranfield, United Kingdom, MK43 0AL.
Email: muhammad.a.khan@cranfield.ac.uk

such as energy absorption, vibration reduction, and buffering (Treviso et al., 2015).

For 3D-printed damping properties, many studies have worked on different materials. Among them, Polylactic Acid (PLA) is widely used in FDM technology nowadays (Lau et al., 2023). In research (He et al., 2023b), the FDM-3D printed pure PLA and ABS underwent dynamic mechanical analysis, and the storage functions of PLA material show reasonable ranges of decent energy absorption characteristics. Besides, it also possesses characteristics like biodegradability, biocompatibility, and mechanical properties to a great extent (Bhayana et al., 2023; Kumar et al., 2022; Rodríguez-Reyna et al., 2022). K. Arunprasath et al. conducted dynamic mechanical analysis on FDM-3D printed PLA and Acrylonitrile Butadiene Styrene (ABS) and studied their interventions. The storage functions of both polymeric materials show an excellent range of decent energy absorption characteristics (Arunprasath et al., 2021). Ge et al. compared the damping behaviour of 3D-printed Tango Black Plus resin with traditional cushioning materials, such as polyethene, under impact loading. The resin showed extreme damping and could absorb almost 100% of the impact energy and recover to the original dimensions after multiple platen drop tests (Ge et al., 2021). Zhang et al. developed a Magnesium-Nitinol (Mg-NiTi) composite using a selective laser melting technique by infiltrating magnesium melt into a 3D-printed Nitinol scaffold. The 3D-printed Mg-NiTi exhibits great damping capacities and exceptional energy absorption efficiency (Zhang et al., 2020).

On the other hand, some studies focused on the influence of printing parameters on damping performance. Previous research has widely investigated that mechanical properties would be influenced by different printing parameter settings (Almutairi et al., 2020; Alshammari et al., 2021; Asif et al., 2019; He et al., 2021b; Mazzanti et al., 2019; Wang et al., 2021). Meanwhile, they also affect damping performance. León-Calero et al. employed compression tests to investigate the specific energy absorption (SEA) and specific damping capacity (SDC) of the 3D-printed thermo-plastic polyurethanes (León-Calero et al., 2021). Francisco Medel et al. proved that natural frequencies of first and second bending modes allowed computation of the corresponding equivalent elastic moduli and identified significant influences of process parameters (raster angle, nozzle temperature, etc.) on mechanical behaviour (Medel et al., 2022). In another paper (Mö et al., 2022), the panels' flexural behaviours and vibration-damping capabilities produced in different infill patterns (grid, cross, and trihexagon) and different infill ratios were investigated. The flexural tests showed that the highest damping capability was obtained on cross-pattern specimens. Similarly, in another research, the effect of different process parameters (nozzle size, infill density, and pattern) on the damping properties (damping ratio and loss factor) for the FDM ABS cantilever beam was also investigated (He et al., 2023a).

Most of the above studies showed that infill patterns could significantly affect the damping properties of the FDM parts. The experimental investigation was performed extensively. However, most of these studies considered different infill patterns as a qualitatively categorised variable. They lacked any discussion on the chosen quantitative geometric features of the pattern and their distinct influence on the obtained damping characteristic. In order to fill the gap, the presented paper aims to work on the effect of the infill pattern's geometric parameters on damping properties. The grid, triangle, and honeycomb infill patterns were investigated with different geometric angles by the experimental works. The experimental results were then used to develop empirical models representing the relationship between the damping properties and infill pattern parameters.

Material and methods

Specimen fabrication

PLA was selected as the raw material for specimen fabrication in this study due to its widespread availability in FDM technology and favourable performance in dynamic mechanical applications (Bhayana et al., 2023; He et al., 2023b; Kumar et al., 2022; Lau et al., 2023; Rodríguez-Reyna et al., 2022). Specifically, PLA offers higher printing stability and lower warpage compared to ABS, ensuring consistent specimen quality. In addition, previous studies have shown that PLA exhibits competitive damping behaviour under dynamic mechanical analysis while maintaining adequate stiffness (Anwer and Naguib, 2016; Ferreira et al., 2021; Pavon et al., 2022), making it particularly suitable for investigating vibration and energy dissipation characteristics in 3D-printed structures.

The specimen was designed as a cantilever beam with the geometry in Figure 1, which is easily printed. It was designed in reference to ASTM E756-05 (2017), which specifies a base beam configuration for vibration-damping measurements. The standard also allows flexibility in beam dimensions and thickness depending on the damping material properties and frequency range of interest. The cantilever structure was used in many studies to simulate some actual applications, such as wind turbine blades and aeroplane wings (Kamei and Khan, 2021; Zai et al., 2019, 2020). It provides an easy-to-measure free vibration response under the impact force. The CAD model of the specimen was designed in SolidWorks and imported into Ultimaker Cura to set the printing parameters. Except for the infill pattern parameters investigated in this work, other printing parameters were set using the same value to ensure the printing quality, as shown in Table 1.

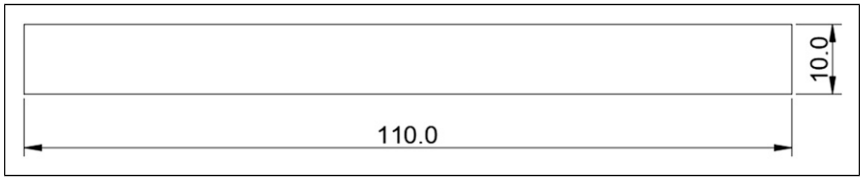

Figure 1. Geometric dimension of the specimen (unit: mm).

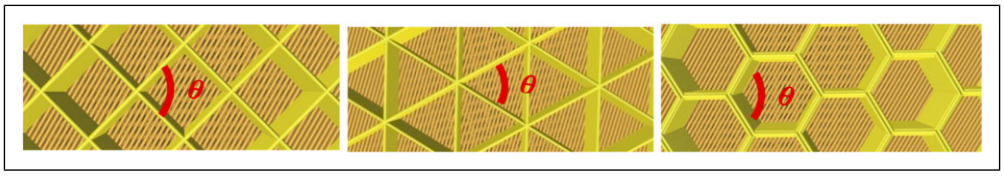

Figure 2. Schematic diagram of the infill line angles in three infill patterns.

Infill pattern determination

Three different infill patterns were investigated in the tests, as shown in Figure 2. The previous paper has proposed that grid and triangle infill patterns affected the damping results (He et al., 2023a). Therefore, these two were selected and tested in specific angle sizes. At the same time, a honeycomb, also called a hexagon infill pattern, was investigated. As one of the advanced structure geometries with lightweight, high stiffness, flexural strength, material utilisation and damping efficiency, it has been widely used in aerospace, the construction industry, shipbuilding, packaging, transportation, and other fields (Wang et al., 2018).

As a quantitative parameter, the angle between the infill lines was investigated for each pattern. There were five levels of angle θ for each pattern from 30 to 150° with a 30° interval. Therefore, the research used a total of 15 structure combinations. For each infill setting, three specimens were printed and tested to ensure the robustness of the results. Figure 3 shows the physical printed specimens.

Experimental setup and procedures

The damping properties of specimens were tested using the impact test following Standard E756 − 05 (2017) (ASTM, 2005). As a cantilever beam, the sample has infinite freedom, which means that there are infinite damping coefficient C_j and damping ratio ξ_j for j^{th} mode. However, this research only focused on the fundamental damping properties. Therefore, the logarithmic decrement method was applied to measure the damping ratio. The testing system is shown in Figure 4, which consists of the accelerometer, the clamp, the data acquisition card, and the chassis.

Table 1. Printing parameter settings.

Printing parameters	Default settings
Layer height	0.1 mm
Wall thickness	0 mm
Nozzle size	0.4 mm
Nozzle temperature	205°C
Nozzle travel speed	40 mm/s

The beam-shaped specimen was horizontally installed on a test bench. A full constraint condition was applied on the beam's fixed end. One accelerometer (PCB 352A21 model, PCB Piezotronics, US) was fixed on the beam's free end, which can monitor the acceleration value. During the experiment, a slight impact force was applied to the beam. Meanwhile, the data was transferred from the accelerometer to the computer by the DAQ card (NI 9234) and DAQ chassis (NI 9174) (National Instrument, UK). The acceleration sensor is connected to the channel signal acquisition analyser through a data cable, and the signal acquisition analyser is connected to a computer equipped with the software SignalExpress through a network cable for recording and displaying vibration measurement signals. SignalExpress saves the acceleration data at each point in time as a text file, which is then imported into MATLAB for processing and analysis.

Data process

The free vibration attenuation method, as an intuitive and simple method, can be used to calculate the damping ratio. When the system vibrates freely, it attenuates exponentially. The attenuation rate δ is defined as the natural logarithm of the ratio of adjacent peaks x_n, x_{n+1}, as shown in equation (1). The fundamental damping ratio ξ is shown in equation (2).

$$\delta \equiv \ln \frac{x_n}{x_{n+1}} = \frac{2\pi\xi}{\sqrt{1-\xi^2}} \approx 2\pi\xi \tag{1}$$

Figure 3. Schematic of the printed specimens with the different infill patterns and infill line angles.

$$\xi = \frac{\delta}{2\pi} \tag{2}$$

Multiple cycles are usually taken into consideration in order to reduce errors. Therefore, the damping ratio can be calculated as shown in equation (3).

$$\xi = \frac{\delta_m}{2\pi m} = \frac{\ln(x_n/x_{n+m})}{2\pi m} \tag{3}$$

The calculated damping ratios were then investigated further by one-way analysis of variance (ANOVA) for each infill pattern to assess whether the variations in damping ratio across different infill angles were statistically significant. The ANOVA method evaluates whether the means of multiple groups differ beyond what would be expected by random chance, thereby validating the role of geometric configuration in influencing damping behaviour.

In addition, the research developed the empirical fitting model to estimate the damping ratio for different infill patterns and angles. The performance of the models can be analysed through the following series of evaluation indicators. The *p*-value serves as a marker of sample confidence. Generally, it is believed that when p<=0.05 (which significance level is generally chosen), there is a chance that the model's signal or the model's results are reliable. R^2 represents the percentage degree of explanation for the relationship between variables and can be used to test the goodness of fit of the overall regression equation. The result is better for R close to value 1 (Zhang et al., 2021).

Results and discussion

Although both the natural frequency and damping ratio can be extracted from the free vibration response, the present study specifically focused on damping behaviour as the primary parameter of interest. The fundamental damping ratios were calculated after the impact tests. Table 2 and Figures 5–7 show the experimental results for the different infill patterns and line angles. All fundamental damping ratios are distributed within the range of 0.008 to 0.02. Both the infill pattern and infill line angles significantly influence damping behaviours.

Influence of the infill pattern on the damping ratio

Even though the distribution range of damping ratios is more consistent across the infill patterns, the average value for each pattern is slightly different. The damping of the triangular structure specimens reaches 0.01162, which is relatively high compared to the other two types. The secondary is the hexagon infill structure, which is 0.01148. In contrast, the average experimental damping ratio of the grid pattern is 0.00951, the lowest among the three.

It suggests that the triangular structure has the best damping performance. Meanwhile, if a better vibration elimination ability is wanted, it is supposed to try to avoid relatively unstable quadrilateral structures. Similar results were also demonstrated in a referenced study (He et al., 2023a).

This result might be possible because triangles are the most stable structures in polygons. This is mainly because the lengths of all three sides are given, and the shape of a triangle is unique. Meanwhile, fewer edges provide a greater concentration of support points. Consequently, the vibration stays on the edges for a shorter time, which may lead to faster stabilisation of the overall structure and higher damping performance. These findings are consistent with previous studies indicating that internal geometry and orientation significantly affect damping performance in FDM-printed cellular structures. Rajpal and Gangadharan (2018) reported that triangular cores exhibited the highest damping ratios compared to grid configurations due to their ability to redistribute stress and enhance deformation paths within the structure.

Influence of the geometric angles on the damping ratio

The statistical significance of geometric angle on damping behaviour was examined using one-way ANOVA, conducted independently for each infill pattern. The results in

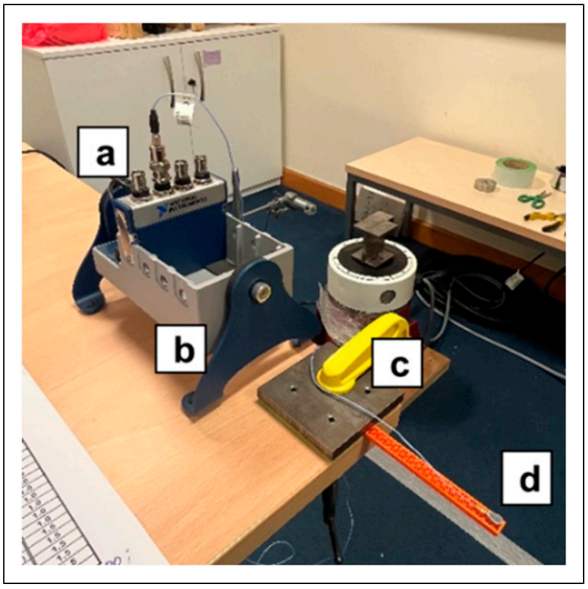

Figure 4. Experimental setup. (a) DAQ card. (b) DAQ chassis. (c) Clamp. (d) Accelerometer.

Table 3 confirmed that the damping ratio differences across different angles were statistically significant in all three infill configurations ($p < 0.05$). Notably, the hexagon and triangle patterns exhibited highly significant p-values (on the order of 10^{-10} to 10^{-15}), indicating a strong dependence of damping characteristics on infill orientation. The grid pattern also showed a statistically significant effect with a comparatively lower F-statistic, 11.73.

The trends significantly differ between the three printing patterns when considering the geometric angles' influence on the damping ratios. One of the critical reasons for this is that the infill density also varies across the geometric angles at the same infill pattern. To illustrate this kind of change, Figure 8 depicts the relationships between the infill density and geometric angles.

In theory, the infill density affects the damping ratio in three ways. Higher infill densities tend to result in an increasing stiffness. It also increases the structure's mass. The internal friction that occurs during the vibration of the increased solid part also dissipates more energy. The combination of these three aspects makes the effect of infill density on the damping ratio particularly complex. This complexity is then coupled with structural differences due to different geometric angles, which influence the final damping ratio together.

Table 2. Damping ratios for different geometric angles with different printing patterns.

Geometric angle (°)	Grid	Triangle	Hexagon
30	0.01015	0.009883	0.015717
60	0.009317	0.0163	0.012317
90	0.008317	0.010183	0.010467
120	0.009467	0.01195	0.009317
150	0.0103	0.009783	0.0096

Grid infill pattern. In the case of the grid infill pattern, which is commonly chosen as the preferred configuration, a distinct trend is observed concerning the damping ratio in Figure 6. Specifically, when considering 90° as the boundary angle, the damping ratio initially decreases from 0.102 to 0.0083 as the angle increases. However, this downward trend shifts, and the value gradually ascends from 90° to 150°. The damping ratio reaches its lowest value of 0.0083 when the grid angle is 90°, the default printing setting.

Meanwhile, it is easy to find that the infill density has the same trend as the outcome with geometric angles changing, which can be observed in Figure 8. The infill density is lowest when the grid's angle is 90°. Previous research (He et al., 2023b) has proved that infill density does have an impact on damping properties. This viewpoint will be discussed quantitatively in [Section 3.2.4], concentrating on the effect of infill density as well.

From a structural mechanics perspective, the sharp decline in the damping ratio at 90° can also be attributed to the internal alignment of printed filaments. At this angle, the grid structure aligns orthogonally with the principal loading directions, resulting in straighter load paths, reduced interlayer shear deformation, and minimal filament junction rotation. This limits the activation of energy dissipation mechanisms such as interfacial friction and micro-sliding. Conversely, at oblique angles (e.g., 60°, 135°), the intersecting load paths introduce more internal deformation zones, frictional interfaces, and filament reorientations, thereby enhancing energy dissipation.

These geometry-dependent damping behaviours are conceptually aligned with Zhang et al. (2015). They demonstrated that optimal damping arises when a structure activates both shear deformation in compliant regions and stress transfer across stiff interfaces. The grid structure disrupts such balance at 90°, leading to minimal energy loss and reduced damping.

Triangle infill pattern. The trend in Figure 5 displays greater fluctuations, particularly regarding the triangle pattern. The damping ratio peaked at 60° when the designs were exactly equilateral triangles, reaching 0.0163. However, contrary to the outcome of the grid pattern, it shows less correlation with the infill density, which demonstrates that geometric angle does affect the damping properties.

The observed diminished relevance in the results could be attributed to the fact that, compared to the other two patterns, the triangular structure incorporates multiple parallel lines aligned with the specimen's wider edge. In research (Zhang et al., 2021), Zhang Heng et al. investigated the damping behaviours using a similar structure with only

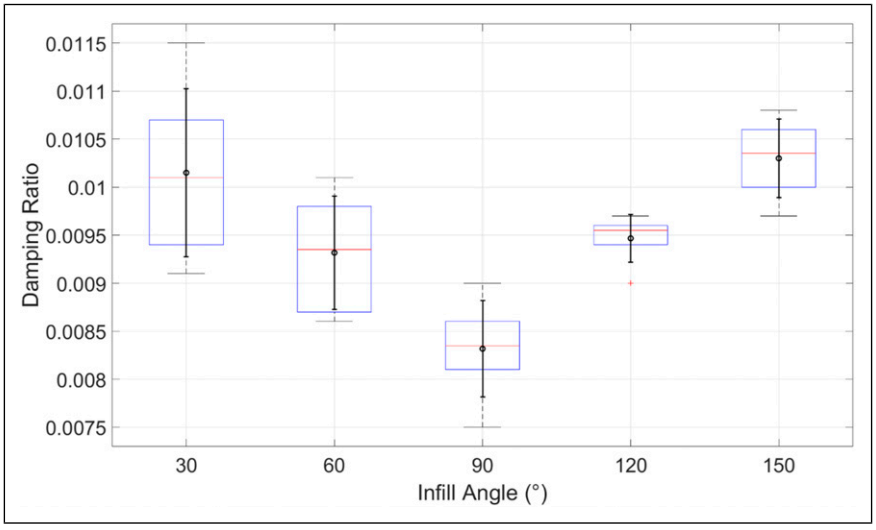

Figure 5. Damping ratios for the grid pattern.

parallel lines. The structure's frequency response gradually decreases with the increase in the damping material's volume fraction. After reaching its minimum value, it gradually rises as the volume fraction increases. This is mainly because the structure's frequency response is related to both the stiffness and damping. Obtaining greater damping at the cost of sacrificing the structural stiffness cannot effectively reduce the structural response. Therefore, for composite structures, there is an optimal stiffness and damping that minimises the structural response.

Applying this concept, it is possible that in the context of the current research, the 60° configuration of the triangular pattern represents an equilibrium point where an optimal balance between stiffness and damping is achieved. Therefore, the fluctuating test results of triangular specimens may be due to the combined effects of angles, similar truss structures parallel to the wide edges, and infill density simultaneously.

Hexagon infill pattern. As shown in Figure 7, the damping ratio trend for the hexagon is similar to the grid pattern, while the trend shift occurs at 120° this time, which is also the default setting angle. The damping ratio also initially experiences a decrease from 0.0157, reaching its minimum value of 0.00932 before a slight increase takes place at 150°.

Compared to the grid, the hexagon pattern exhibits angled intersections and multi-directional connectivity even at default settings. At 120°, the filaments are highly ordered, resulting in lower shear activation. As the angle shifts to 150°, oblique paths increase internal shear and micro-

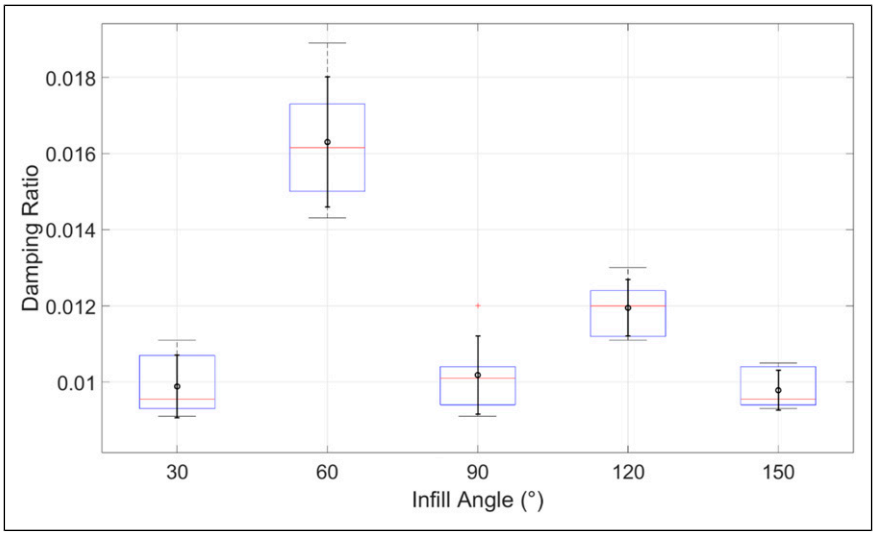

Figure 6. Damping ratios for the triangle pattern.

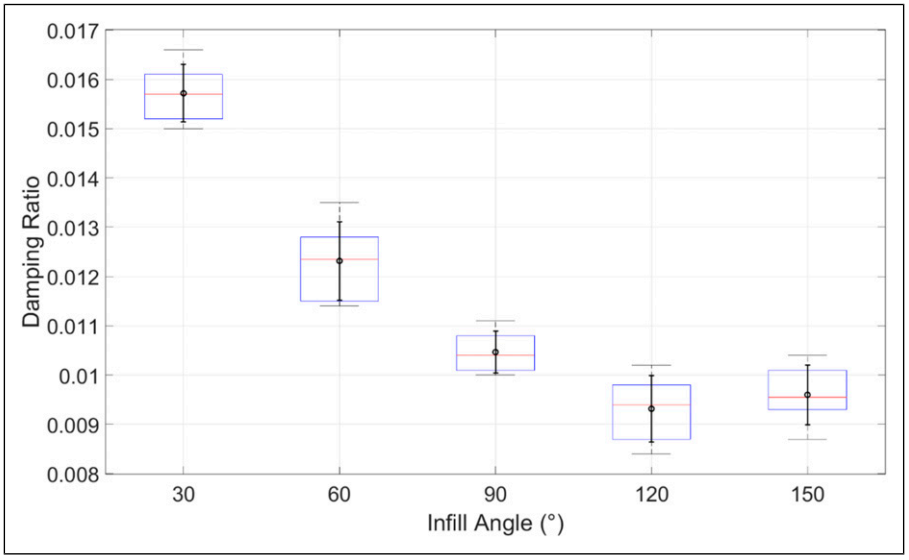

Figure 7. Damping ratio for hexagon pattern.

friction, explaining the partial recovery in damping ratio. This behaviour is consistent with the underlying mechanisms described by Zhang et al. (2015), where a staggered, geometry-driven distribution of deformation can optimise the balance between stiffness and damping. In the hexagonal pattern, the energy dissipation is governed by the degree to which filament paths are redirected and shear deformation zones are activated – a strongly angle-dependent effect.

This trend also corresponds to the infill density change in Figure 8, which is discussed in detail in Section 3.2.4. Therefore, for honeycomb infill structures that do not have parallel lines in the same direction as wide edges, there is a high possibility that the infill density remains the dominant factor affecting damping performance.

Influence of the infill density on the damping ratio. As the geometric angles of each filling pattern change, the coverage of the infill density changes within the range of approximately 25% to 70%. In the case of the grid infill pattern structure, with the geometric angle progressively increasing from 30° to 90°, the infill density of the specimen drops from 46.85% to 32.97%. This reduction contributes to a decrease in stiffness. Subsequently, as the angle continues to increase, the density rises, leading to a subsequent recovery in stiffness. This dynamic interplay has a corresponding influence on the trend observed in the damping ratio.

The infill density of hexagonal structural specimens also changes with a similar variation process. The value decreased from 40.20%, reaching the lowest value of 26.35% at an angle of 120°, and finally increased slightly to 28.46%. This trend also aligns with the damping ratio change.

However, the damping ratio of the triangle pattern's structure performs a highly non-linear relationship with the infill density. 60° geometric angle introduces a slightly lowest infill density 42.96%, which is similar to 90° geometric angle's 43.24%. However, these two specimens have a significant difference in the damping ratio results. From another perspective, this phenomenon demonstrates that the infill density and the geometric angles have a combined influence on the damping performance.

Empirical modelling and validation

Empirical model development. Since the relationship between the damping ratio and the geometric angles for the grid and hexagon patterns is significant, this research assessed their interaction using a quadratic polynomial regression model shown in equation (4). The fitting coefficients and R-square values are shown in Table 4.

$$\xi = p_0 x^2 + p_1 x + p_2 \tag{4}$$

To quantify the reliability and stability of the polynomial regression models, 95% confidence intervals (CIs) were computed for all model parameters. All fitted coefficients exhibited narrow confidence intervals that did not include zero, confirming their statistical significance.

Table 3. One-way ANOVA results.

Pattern	F-statistic	*p*-value
Triangle	41.57	1.07×10^{-10}
Grid	11.73	1.68×10^{-5}
Hexagon	105.66	2.78×10^{-15}

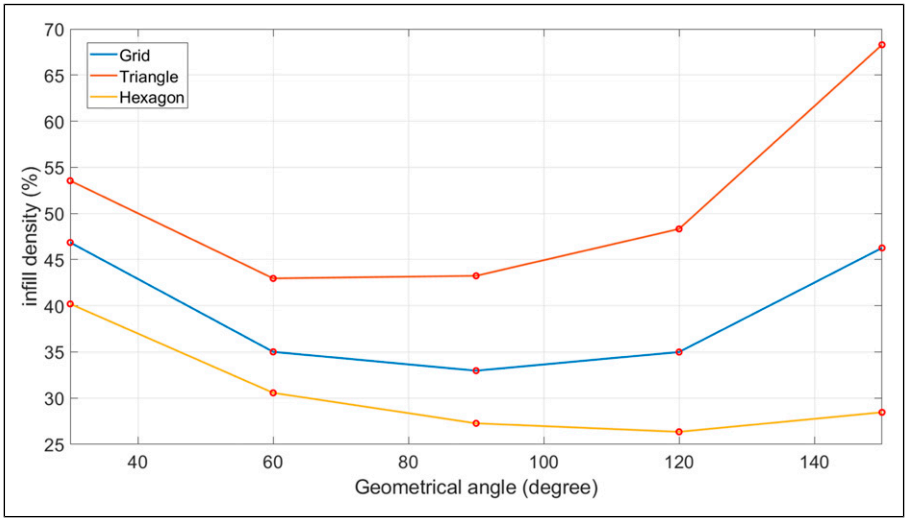

Figure 8. Infill densities of different geometric angles.

Table 4. Model coefficients and R-square value. Values in parentheses indicate the 95% confidence intervals for each parameter.

Infill pattern	p_0	p_1	p_2	R^2
Grid	$4.352*10^{-7}$ ($2.91*10^{-7}$, $5.80*10^{-7}$)	$-7.683*10^{-5}$ ($-1.03*10^{-4}$, $-5.04*10^{-5}$)	0.01212 ($1.11*10^{-2}$, $1.32*10^{-2}$)	0.8682
Hexagon	$6.402*10^{-7}$ ($4.95*10^{-7}$, $7.86*10^{-7}$)	$-1.66*10^{-4}$ ($-1.93*10^{-4}$, $-1.39*10^{-4}$)	0.02009 (0.0190, 0.0211)	0.9429

Validation. The fitting curve has been derived for each pattern, utilising experimental data as a basis, as depicted in Figure 9. To validate them, specimens at four distinct angles (45°, 75°, 105°, and 135°) were printed and subjected to identical testing procedures. These angles were not included in the original model fitting dataset to ensure independent validation. The validation data points, marked in red, have been incorporated into the figure.

The errors of four validations can be obtained by contrasting the model results with the experimental data, shown in Table 5. Figure 9 and table indicate that the validation

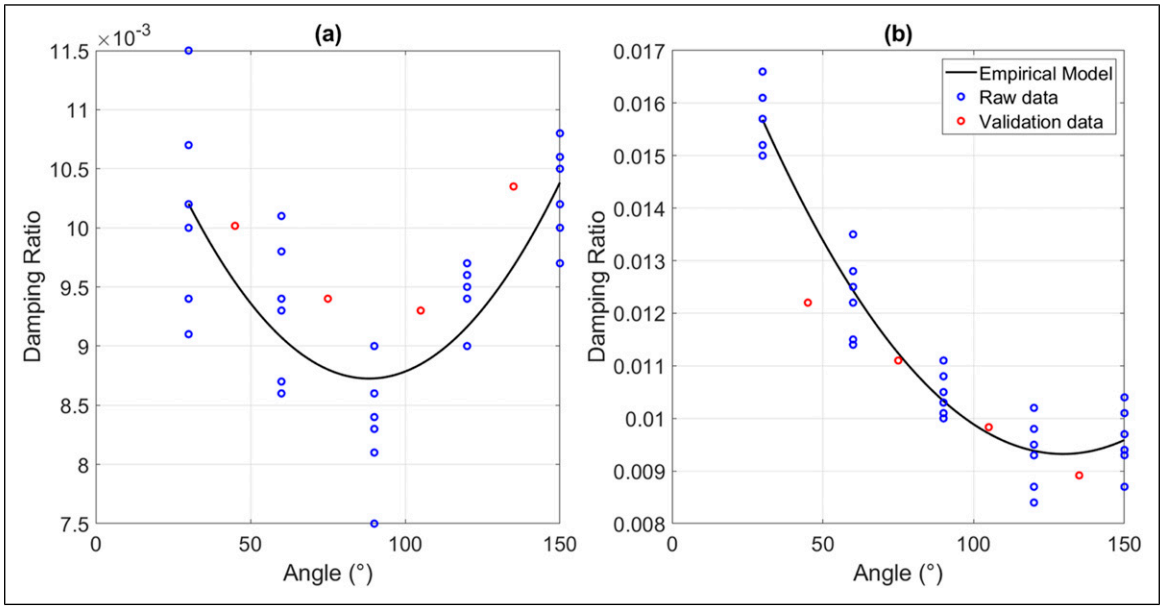

Figure 9. Experimental results and empirical model: (a) Grid pattern and (b) hexagon pattern.

Table 5. Model estimations and their differences with the experimental validation results.

Printing pattern	Geometric angle (°)	45	75	105	135
Grid	Test results	0.0100	0.0094	0.0093	0.0104
	Empirical model results	0.00954	0.00880	0.00885	0.00968
	Relative difference	−4.75%	−6.36%	−4.87%	−6.52%
Hexagon	Test results	0.0122	0.0111	0.009833	0.008917
	Empirical model results	0.0139	0.0112	0.00971	0.00934
	Relative difference	14.04%	1.23%	−1.22%	4.77%

experiment results of both grid and hexagonal infill patterns are also comparatively ideal.

In the grid pattern case, it is worth mentioning that even though the model trend is reasonable, it has underestimated results compared to the practical damping ratio for all validations. Further dataset is still required to investigate the phenomenon. On the other hand, except for a relatively large deviation of 45° filament angle, the experimental and model results of the remaining hexagonal specimens are relatively close.

Conclusions

This research investigated the effect of structural and geometrical infill pattern parameters on the FDM PLA's damping properties. It proposes the quantitative study for geometric attributes of infill patterns and assessing their impact on damping behaviours for the first time as a new dimension to the analysis of FDM polymeric material damping performance, which filled in the gap that previous research only focused on investigating the effect of the default infill patterns.

Both infill patterns and geometric angles affect the fundamental damping ratios. The extreme values of the damping ratio all occur at the default pattern angles. 60° triangle infill pattern reaches the highest damping ratio, 0.0163, in all tests. In addition, infill density change due to various geometric angles also plays a vital role in damping properties. The damping ratios are linearly related to the infill density in the grid and hexagon infill pattern. Therefore, the empirical damping ratio prediction model for the grid and hexagon infill patterns was developed and validated based on the experimental data. The regression yielded high R^2 values of 0.8682 and 0.9429, respectively, which statistically confirms the strong dependence of the damping ratio on infill line angle. These relationships provide a basis and guidance for selecting and manufacturing specific damping ratio structures.

The significance of the research reveals that without altering external dimensions, the adjustments to FDM material's infill parameters enable the tailored control of damping characteristics to meet specific needs. The outcomes provide a tool for designing customised damping materials. Future work could explore the generalisability of the observed geometric-damping relationships to other polymeric materials, including flexible or viscoelastic filaments such as TPU, which may exhibit higher damping capacity – as well as to more complex or bio-inspired infill structures, to enhance vibration control capabilities further. In addition, future research could integrate structural mechanics principles and material constitutive behaviour into modelling, enabling better physical interpretability and improved damping behaviour predictive capability across a wider range of design configurations and materials.

ORCID iDs

Feiyang He https://orcid.org/0000-0002-4457-4343
Muhammad Khan https://orcid.org/0000-0001-9028-1288

Funding

The authors received no financial support for the research, authorship, and/or publication of this article.

Declaration of conflicting interests

The authors declared no potential conflicts of interest with respect to the research, authorship, and/or publication of this article.

References

Abusabir A, Khan MA, Asif M, et al. (2022) Effect of architected structural members on the viscoelastic response of 3D printed simple cubic lattice structures. *Polymers* 14(3): 618.

Aimar A, Palermo A and Innocenti B (2019) The role of 3D printing in medical applications: a state of the art. *Journal of Healthcare Engineering* 2019: 1.

Almutairi MD, Aria AI, Thakur VK, et al. (2020) Self-healing mechanisms for 3D-printed polymeric structures: from lab to reality. *Polymers* 12: 1534.

Almutairi MD, Mascarenhas TA, Alnahdi SS, et al. (2023) Modal response of hybrid raster orientation on material extrusion printed acrylonitrile butadiene styrene and polyethylene terephthalate glycol under thermo-mechanical loads. *Polymer Testing* 120: 107953.

Alshammari YLA, He F and Khan MA (2021) Modelling and investigation of crack growth for 3D-Printed acrylonitrile butadiene styrene (ABS) with various printing parameters and ambient temperatures. *Polymers* 13(21): 3737.

Anwer MAS and Naguib HE (2016) Study on the morphological, dynamic mechanical and thermal properties of PLA carbon nanofibre composites. *Composites Part B: Engineering* 91: 631–639.

Arunprasath K, Vijayakumar M, Ramarao M, et al. (2021) Dynamic mechanical analysis performance of pure 3D printed

polylactic acid (PLA) and acrylonitrile butadiene styrene (ABS). *Materials Today: Proceedings* 50: 1559.

Asif M, Ramezani M, Khan KA, et al. (2019) Experimental and numerical study of the effect of silica filler on the tensile strength of a 3D-printed particulate nanocomposite. *Comptes Rendus Mecanique* 347(9): 615–625.

Asli S, Khan B and Potential M (2024) Potential of non-contact dynamic response measurements for predicting small size or hidden damages in highly damped structures. *Sensors* 24: 5871.

ASTM (2005) Standard test method for measuring vibration-damping properties of materials. *Annual Book of ASTM Standards* 04.06: 1.

Atwah AA and Khan MA (2023) Influence of microscopic features on the self-cleaning ability of textile fabrics. *Textile Research Journal* 93: 450.

Atwah AA, Almutairi MD, He F, et al. (2022) Influence of printing parameters on self-cleaning properties of 3D printed polymeric fabrics. *Polymers* 14(15): 3128.

Azouz Z, Honarvar Shakibaei Asli B and Khan M (2023) Evolution of crack analysis in structures using image processing technique: a review. *Electronics* 12(18): 3862.

Baqasah HI, He F, Khan MA, et al. (2019b) Vibration monitoring for in-situ health assessment of 3D printed polymer structure. In: 58th Annual Conference of the British Institute of Non-Destructive Testing, NDT 2019, 1 - *3 September 2019*, The international centre, Telford United Kingdom.

Baqasah H, He F, Zai BA, et al. (2019a) In-situ dynamic response measurement for damage quantification of 3D printed ABS cantilever beam under thermomechanical load. *Polymers* 11(12): 2079.

Bhayana M, Singh J, Sharma A, et al. (2023) A review on optimized FDM 3D printed Wood/PLA bio composite material characteristics. *Materials Today: Proceedings*.

Chan KP, He F, Atwah AA, et al. (2023) Experimental investigation of self-cleaning behaviour of 3D-printed textile fabrics with various printing parameters. *Polymer Testing* 119: 107941.

Deswal S, Kaushik A, Garg RK, et al. (2024) Optimization of fused deposition modelling printing parameters using hybrid GA-fuzzy evolutionary algorithm. *Sādhanā* 49(4): 1–17.

Ferreira M, Peixinho N, Carneiro V, et al. (2021) Stiffness and damping properties of a composite beam design. *Advanced Structured Materials* 149: 101–109.

Francese A, Khan M and He F (2023) Role of dynamic response in inclined transverse crack inspection for 3D-Printed polymeric beam with metal stiffener. *Materials* 16(8): 3095.

Fundamental M, Cadini F, Ribeiro D, et al. (2024) Fundamental challenges and complexities of damage identification from dynamic response in plate structures. *Applied Sciences* 14: 8230.

Ge C, Cormier D and Rice B (2021) Damping and cushioning characteristics of polyjet 3D printed photopolymer with kelvin model. *Journal of Cellular Plastics* 57(4): 517–534.

Hassanieh SA, Alhantoobi A, Khan KA, et al. (2021) Mechanical properties and energy absorption characteristics of additively manufactured lightweight novel re-entrant plate-based lattice structures. *Polymers* 13(22): 3882.

He F, Alshammari YLA and Khan M (2021b) The effect of printing parameters on crack growth rate of FDM ABS cantilever beam under thermo-mechanical loads. *Procedia Structural Integrity* 34: 59.

He F and Khan M (2021) Effects of printing parameters on the fatigue behaviour of 3D-Printed ABS under dynamic thermo-mechanical loads. *Polymers* 13(14): 2362.

He F, Thakur VK and Khan M (2021a) Evolution and new Horizons in modeling crack mechanics of 3D printing polymeric structures. *Materials Today Chemistry* 20: 100393.

He F, Khan M and Aldosari S (2022) Interdependencies between dynamic response and crack growth in a 3D-Printed acrylonitrile butadiene styrene (ABS) cantilever beam under thermo-mechanical loads. *Polymers* 14(5): 982.

He F, Ning H and Khan M (2023a) Effect of 3D printing process parameters on damping characteristic of cantilever beams fabricated using material extrusion. *Polymers* 15(2): 257.

He F, Xu C and Khan M (2023b) Tribological characterisation and modelling for the fused deposition modelling of polymeric structures under lubrication conditions. *Polymers* 15(20): 4112.

Joshi SC and Sheikh AA (2015) 3D printing in aerospace and its long-term sustainability. *Virtual and Physical Prototyping* 10(4): 175–185.

Kamei Khangamlung K and Khan Muhammad M (2021) Current challenges in modelling vibrational fatigue and fracture of structures: A review. *Journal of the Brazilian Society of Mechanical Sciences and Engineering* 43(2).

Kaushik A and Garg RK (2023) Effect of printing parameters on the surface roughness and dimensional accuracy of digital light processing fabricated parts. *Journal of Materials Engineering and Performance*. Epub ahead of print 2023.

Kaushik A, Kumar P, Gahletia S, et al. (2023) Optimization of dual extrusion fused filament fabrication process parameters for 3D printed nylon-reinforced composites: pathway to Mobile and transportation revolution. *SAE International Journal of Materials and Manufacturing* 17(1): 3–18.

Kumar R, Sharma H, Saran C, et al. (2022) A comparative study on the life cycle assessment of a 3D printed product with PLA, ABS & PETG materials. *Procedia CIRP* 107: 15.

Lau HY, Hussin MS, Hamat S, et al. (2023) Effect of kenaf fiber loading on the tensile properties of 3D printing PLA filament. *Materials Today: Proceedings*.

León-Calero M, Reyburn Valés SC, Marcos-Fernández Á, et al. (2021) 3D printing of thermoplastic elastomers: role of the chemical composition and printing parameters in the production of parts with controlled energy absorption and damping capacity. *Polymers* 13(20): 3551.

Li Y, Yang H, Wiercigroch M, et al. (2023) Bionic structure inspired by tree frogs to enhance damping performance. *ACS Applied Materials and Interfaces* 15(26): 31979–31993.

Mazzanti V, Malagutti L and Mollica F (2019) FDM 3D printing of polymers containing natural fillers: a review of their mechanical properties. *Polymers* 11(7): 1094.

Medel F, Abad J and Esteban V (2022) Stiffness and damping behavior of 3D printed specimens. *Polymer Testing* 109: 107529.

Mö Ö, Çakir FH and Sofuoğlu MA (2022) Effect of infill pattern and ratio on the flexural and vibration damping characteristics of FDM printed PLA specimens. *Materials Today Communications* 33: 104912.

Narang R, Kaushik A, Dhingra AK, et al. (2024) Post-treatment and hybrid techniques for prolonging the service life of fused deposition modeling printed automotive parts: a wear strength perspective. SAE international journal of materials and manufacturing 17. *SAE International Journal of Materials and Manufacturing* 17(2): 193–209.

Pavon C, Aldas M, Samper MD, et al. (2022) Mechanical, dynamic-mechanical, thermal and decomposition behavior of 3D-Printed PLA reinforced with CaCO3 fillers from natural resources. *Polymers* 14(13): 2646.

Rajpal RKPL and Gangadharan KV (2018) Parametric studies on bending stiffness and damping ratio of sandwich structures. *Additive Manufacturing* 22: 583.

Rodríguez-Reyna SL, Mata C, Díaz-Aguilera JH, et al. (2022) Mechanical properties optimization for PLA, ABS and nylon + CF manufactured by 3D FDM printing. *Materials Today Communications* 33: 104774.

Shams H, Basit K, Khan MA, et al. (2021a) Realizing surface amphiphobicity using 3D printing techniques: a critical move towards manufacturing low-cost reentrant geometries. *Additive Manufacturing* 38: 101777.

Shams H, Basit K, Khan MA, et al. (2021b) Scalable wear resistant 3D printed slippery liquid infused porous surfaces (SLIPS). *Additive Manufacturing* 48: 102379.

Torrado AR, Shemelya CM, English JD, et al. (2015) Characterizing the effect of additives to ABS on the mechanical property anisotropy of specimens fabricated by material extrusion 3D printing. *Additive Manufacturing* 6: 16–29.

Treviso A, Van Genechten B, Mundo D, et al. (2015) Damping in composite materials: properties and models. *Composites Part B: Engineering* 78: 144–152.

Vanaei HR, Khelladi S and Tcharkhtchi A (2022) Strain release behaviour during crack growth of a polymeric beam under elastic loads for self-healing. *Polymers* 14: 3102.

Wang D, Bai Z and Liao Q (2018) 3D energy absorption diagram construction of paper honeycomb sandwich panel. *Shock and Vibration* 2018: 4067062.

Wang P, Zou B, Ding S, et al. (2021) Effects of FDM-3D printing parameters on mechanical properties and microstructure of CF/PEEK and GF/PEEK. *Chinese Journal of Aeronautics* 34(9): 236–246.

Zai BA, Khan M, Khan KA, et al. (2019) The role of dynamic response parameters in damage prediction. *Proceedings of the Institution of Mechanical Engineers - Part C: Journal of Mechanical Engineering Science* 233(13): 4620–4636.

Zai BA, Khan MA, Khan KA, et al. (2020) A novel approach for damage quantification using the dynamic response of a metallic beam under thermo-mechanical loads. *Journal of Sound and Vibration* 469: 115134.

Zhang P, Heyne MA and To AC (2015) Biomimetic staggered composites with highly enhanced energy dissipation: modeling, 3D printing, and testing. *Journal of the Mechanics and Physics of Solids* 83: 285–300.

Zhang M, Yu Q, Liu Z, et al. (2020) 3D printed Mg-NiTi interpenetrating-phase composites with high strength, damping capacity, and energy absorption efficiency. *Science Advances* 6(19): eaba5581.

Zhang H, Ding X, Shen L, et al. (2021) Topology optimization of sandwich damping composite structure with connective constraint. *Zhongguo Jixie Gongcheng/China Mechanical Engineering* 32(20): 2403.

Damping characterisation for 3D-printed polymeric structure with different geometric parameters

He, Feiyang

2025-12-31

He F, Fan W, Khan M. (2025) Damping characterisation for 3D-printed polymeric structure with different geometric parameters. Journal of Vibration and Control, Avaliable online 15 October 2025 https://doi.org/10.1177/10775463251387454